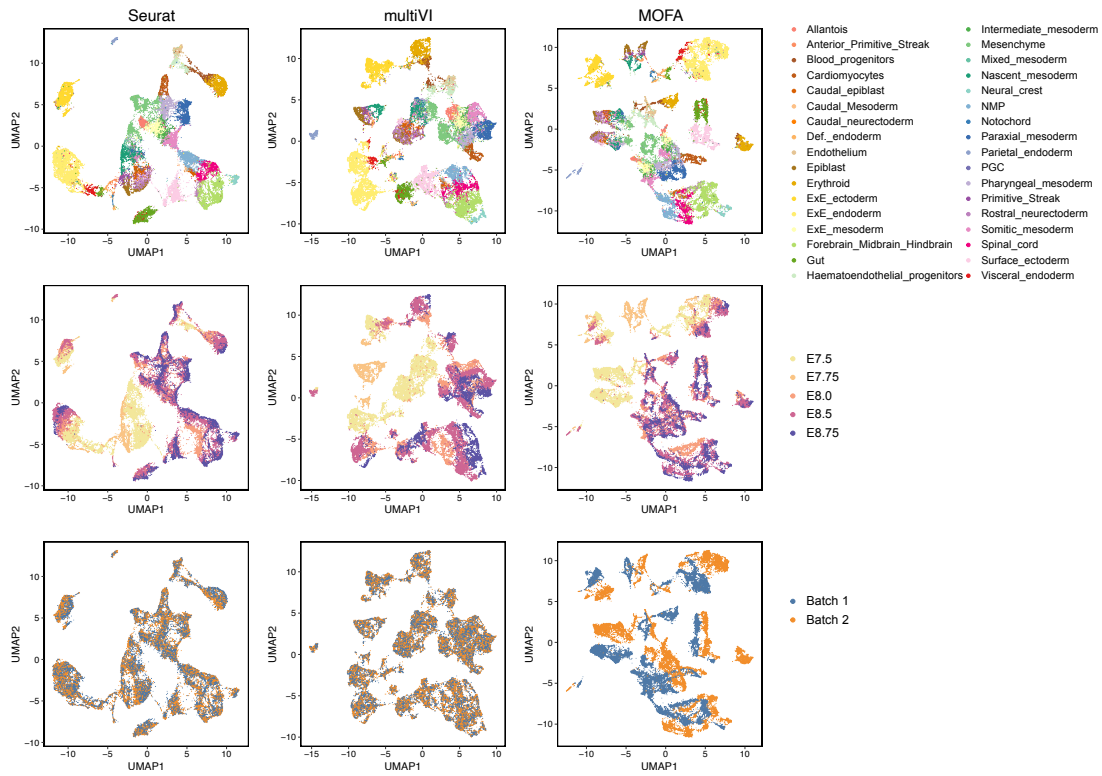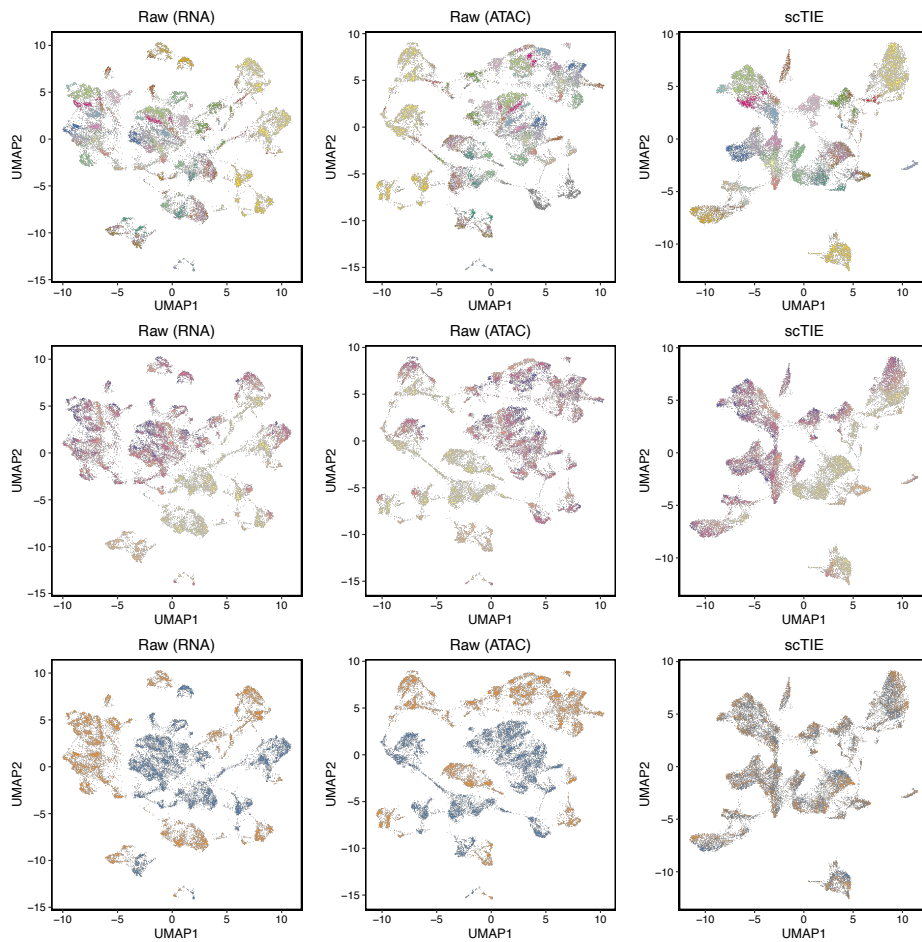# Supplemental Materials

Supplementary Figure S1: Joint visualization using UMAP of the synthetic dataset with batch effect in RNA and noise in ATAC for three data integration methods (Seurat, multiVI and MOFA), colored by cell type annotations (first row), sampling day (second row) and synthetic batch information (third row). Each dot represents a cell in the embedding space.
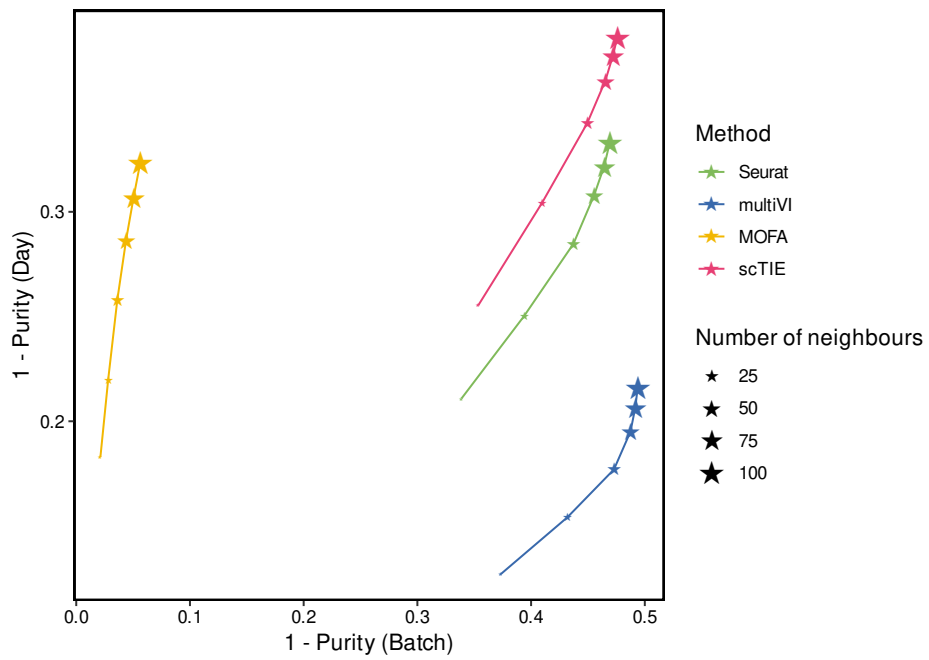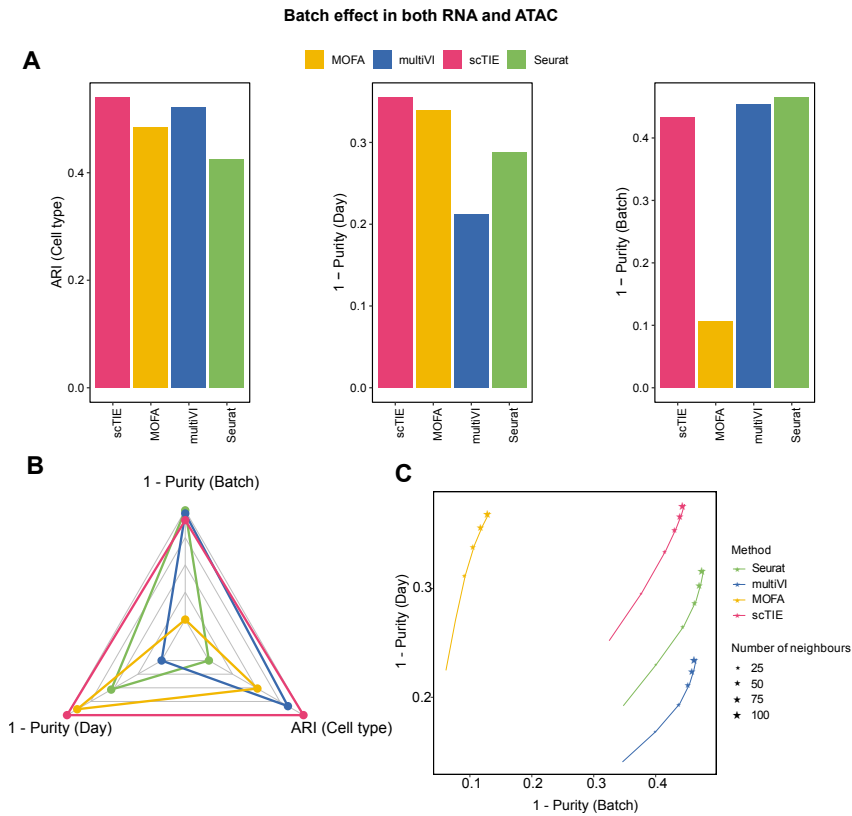
Supplementary Figure S2: Scatter plot showing 1 - average purity scores of batch (x-axis) versus 1 - average purity scores of sampling day (y-axis) as the number of neighbors changes, where the size of stars represents the number of neighbors and color of the stars represents the method. Points in the top right corner have better day alignment and batch mixing.
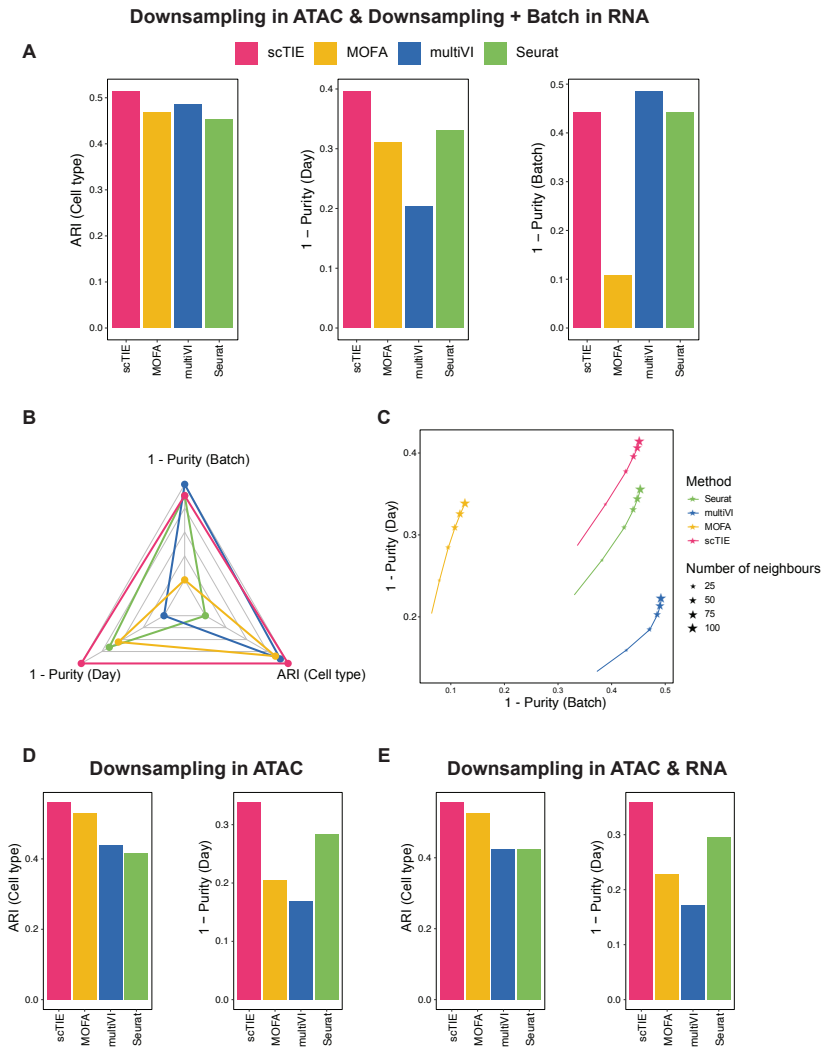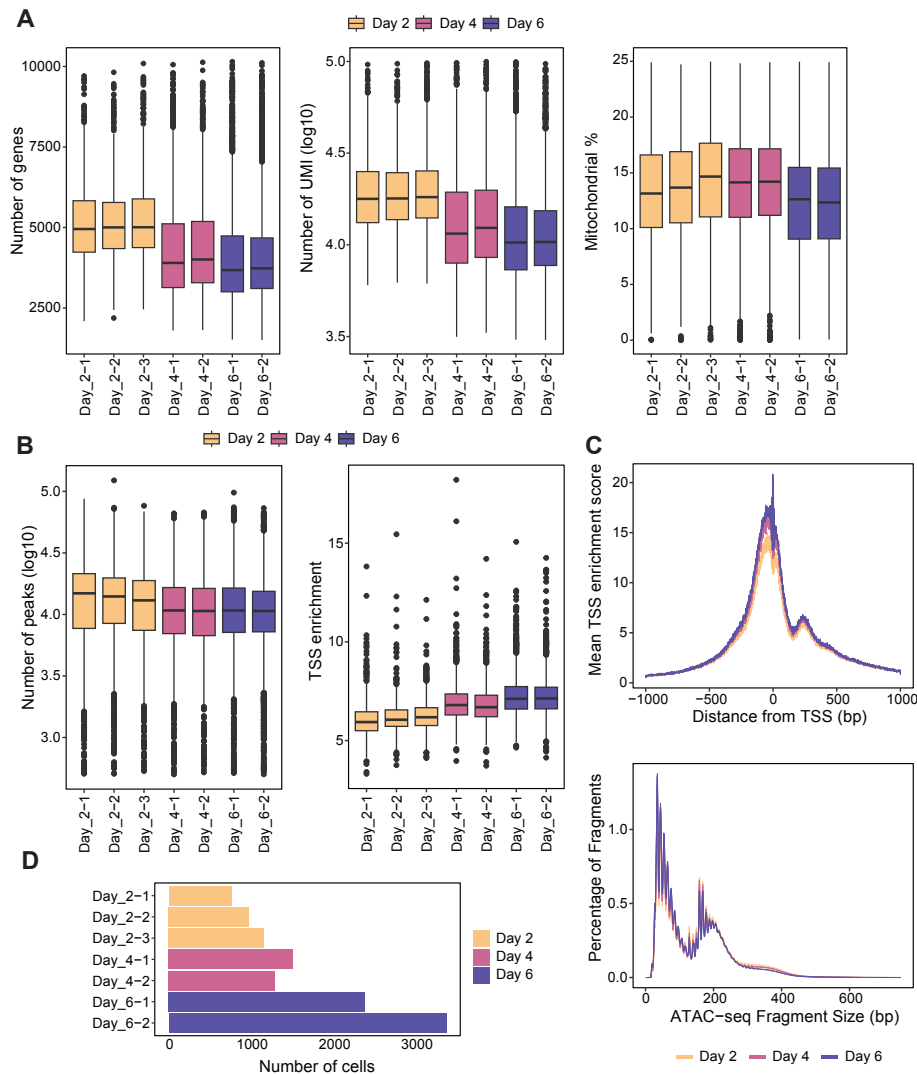
Supplementary Figure S3: Evaluation results for variations of synthetic data settings: (A-C) Read downsampling in ATAC & Read downsampling + Batch effect in RNA: (A) Bar plots showing the evaluation metrics of different data integration methods, including ARI values for clustering with annotations (left); 1 - average purity scores of sampling day (middle) and 1 - average purity scores of the synthetic batch (right). (B) Radar plot summarizing the three evaluation metrics shown in (A), where each line represents the performance of one method, and each axis represents an evaluation metric, starting from the minimum value of all methods. (C) Scatter plot showing 1 - average purity scores of batch (x-axis) versus 1 - average purity scores of sampling day (y-axis) as the number of neighbors changes, where the size of stars represents the number of neighbors and color of the stars represents the method. (D-E) Bar plots showing the evaluation metrics of different data integration methods, including ARI values for clustering with annotations (left); 1 - average purity scores of sampling day (right) for (D) Read downsampling in ATAC and (E) Read downsampling in both ATAC and RNA.

Supplementary Figure S4: Visualization using UMAP of the synthetic dataset with batch effects in both RNA and ATAC data for raw RNA, ATAC and scTIE output, colored by cell type annotations (first row), sampling days (second row) and synthetic batch information (third row). Each dot represents a cell in the embedding space.

Supplementary Figure S5: Evaluation results for synthetic data settings with batch effect in both RNA and ATAC: (A) Bar plots showing the evaluation metrics of different data integration methods, including ARI values for clustering with annotations (left); 1 - average purity scores of sampling day (middle) and 1 - average purity scores of the synthetic batch (right). (B) Radar plot summarizing the three evaluation metrics shown in (A), where each line represents the performance of one method, and each axis represents an evaluation metric, starting from the minimum value of all methods. (C) Scatter plot showing 1 - average purity scores of batch (x-axis) versus 1 - average purity scores of sampling day (y-axis) as the number of neighbors changes, where the size of stars represents the number of neighbors and color of the stars represents the method.

Supplementary Figure S6: (A) Box plots showing the distribution of RNA quality metrics of each sample, colored by the sampling day, including number of genes detected (left), number of total UMI (log10) (middle) and Mitochondrial (MT) gene fraction per cell (right). (B) Box plots showing the distribution of ATAC quality metrics of each sample, colored by the sampling day, including number of peaks detected ($\log_{10}$) (left) and transcription start site (TSS) enrichment (middle). (C) Line plot showing the distribution of ATAC quality metrics of each sample, colored by sampling day, including normalized TSS enrichment score of each sample at each position relative to the TSS (first row) and fragment size distribution (second row). (D) Bar plots indicates the number of cells after quality control in each sample, colored by sampling day.

Reference using Mittnenzweig et al.
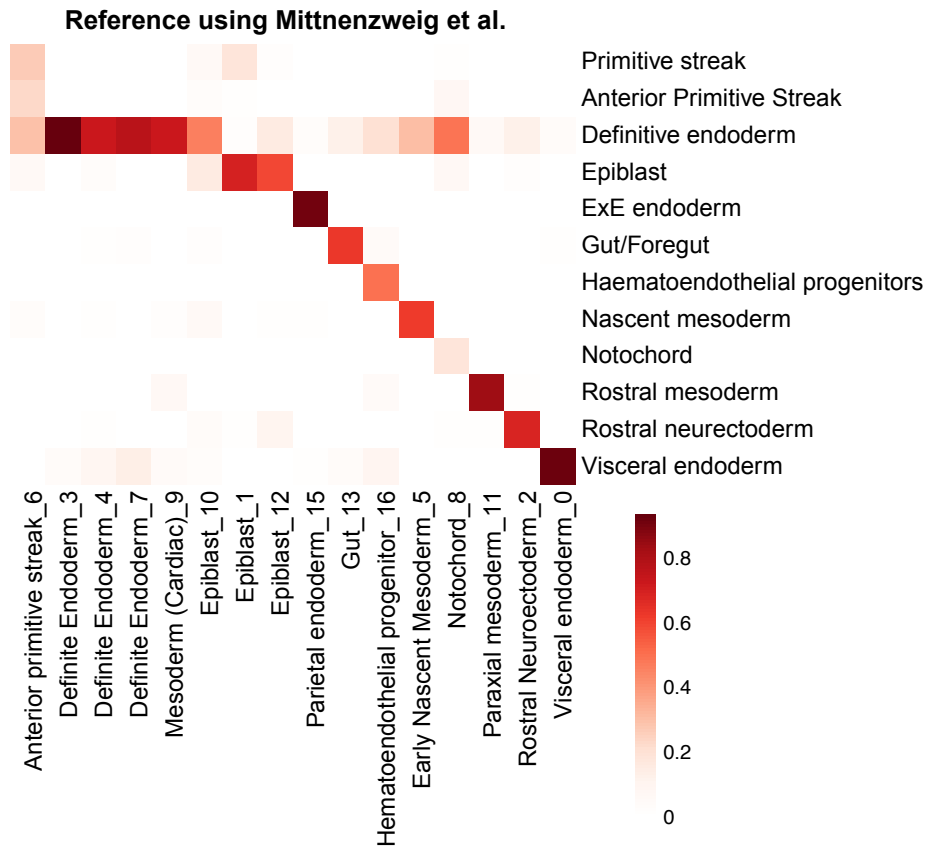
Supplementary Figure S7: Heatmap comparing the clustering results and the transferred labels by scClassify (Y Lin et al. 2020) using Mittnenzweig data as reference (Mittnenzweig et al. 2021). Color indicates the proportion of cells classified as a certain cell type label in the reference for one cluster.
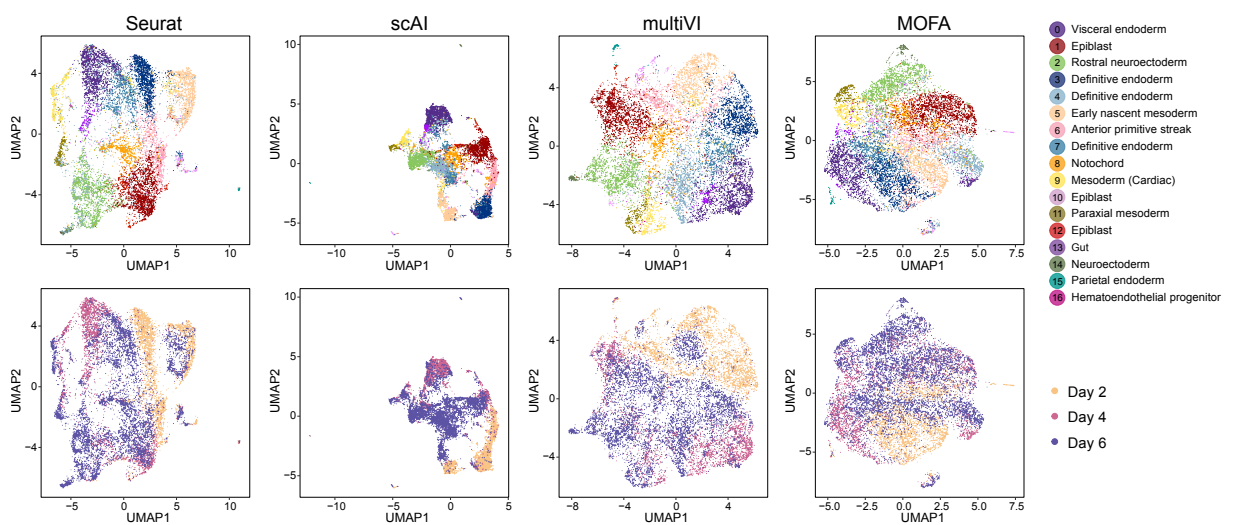

Supplementary Figure S8: UMAP visualization of the mESC dataset for Seurat, scAI, multiVI and MOFA, colored by annotated cell types (first row) and sampling days (second row).
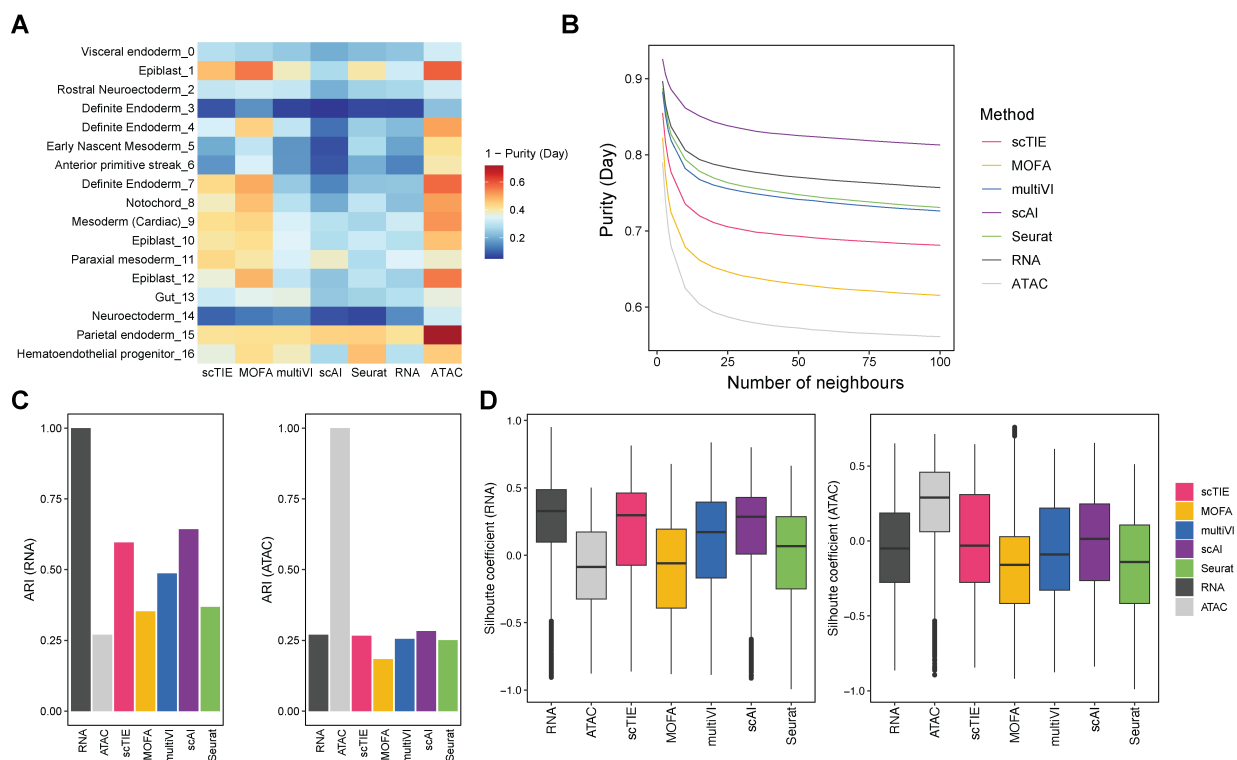
Supplementary Figure S9: (A) 1 - Average purity scores of sampling day for each cell type (Number of neighbors = 50). Row indicates cell types and column indicates methods. Higher values indicate better mixing between days. (B) Average purity scores of sampling day based on different number of neighbors, colored by different methods. Lower values indicate better mixing between days. (C) The bar plots show the ARI values comparing the clustering from different data integration methods with clustering on RNA (left) and ATAC alone (right); higher values indicate better agreement. Note that here RNA and ATAC clustering results are the ground truth for the left panel and right panel respectively, therefore they have ARI equal to 1. (D) Box plots show the silhouette coefficient comparing the clustering from different data integration methods based on distance matrices computed from the RNA (left) and ATAC (right) UMAP coordinates. Higher values indicate better agreement. Note that for the left panel, RNA clustering result has the highest silhouette coefficients because clustering derived from RNA is used as the ground truth; similarly for the right panel.
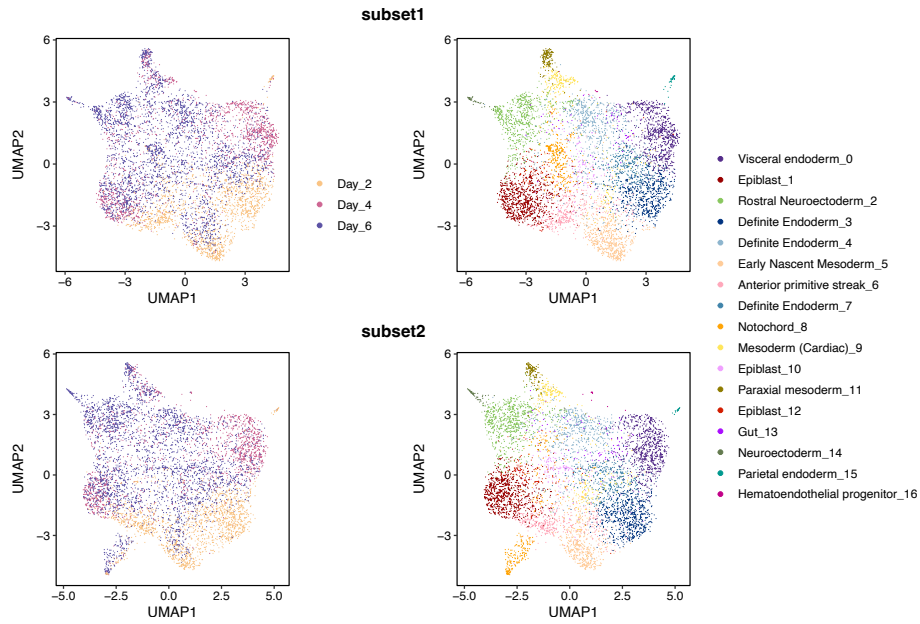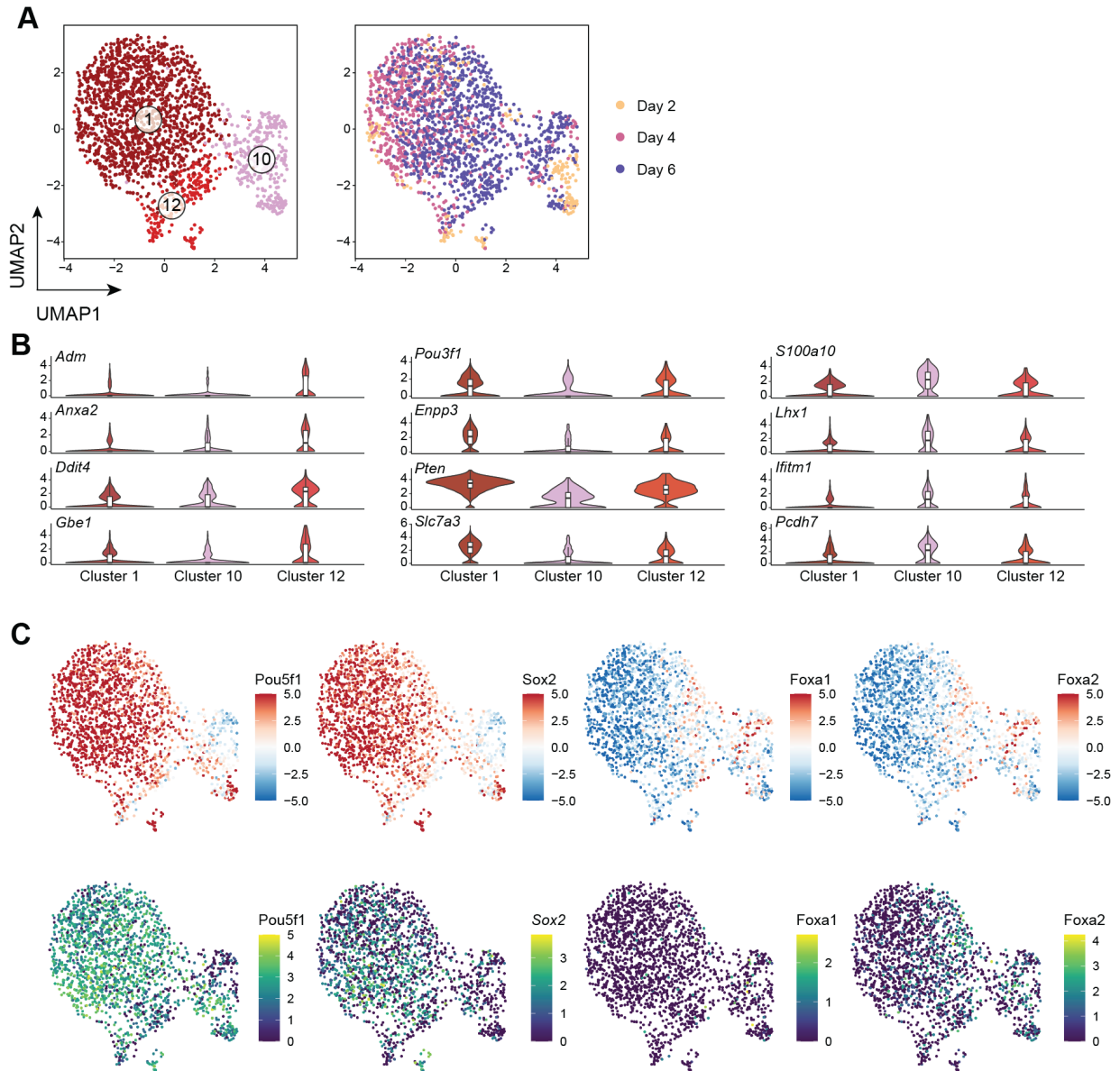
Supplementary Figure S10: UMAP visualizations for the two subsets considered as pseudo-replicates of the mESC dataset.
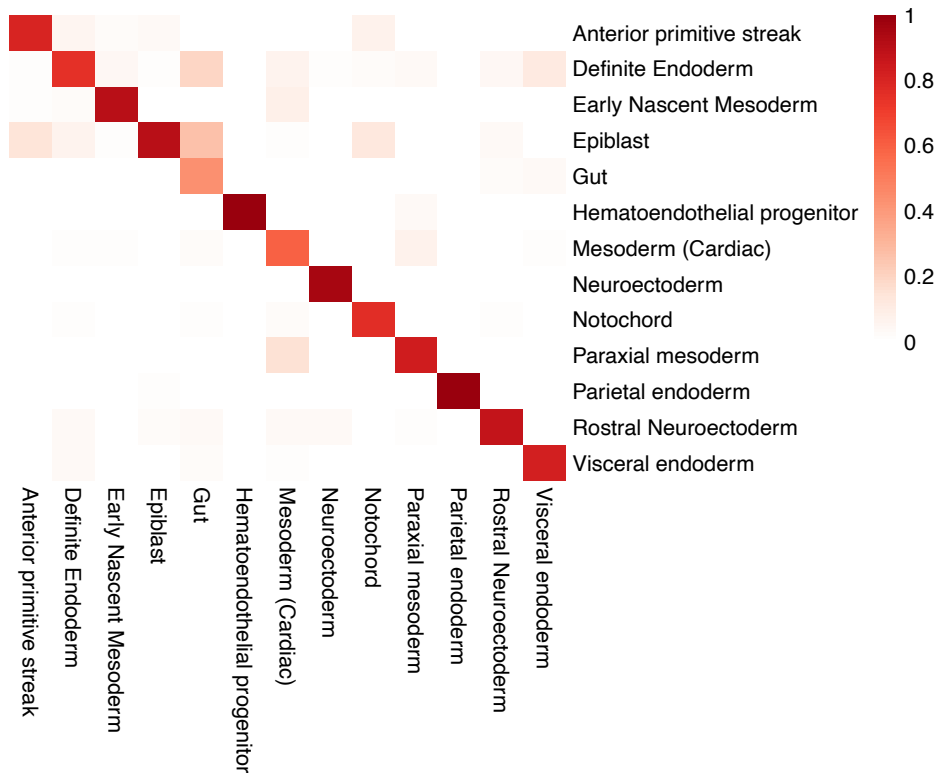

Supplementary Figure S11: Comparison of annotations from the complete dataset (row) with those from the subsets (column). Each entry (i, j) in the heatmap shows the percentage of cells from cell type j (annotated from the subsets) labeled as cell type i in the complete data. The overall accuracy rate is 81%.
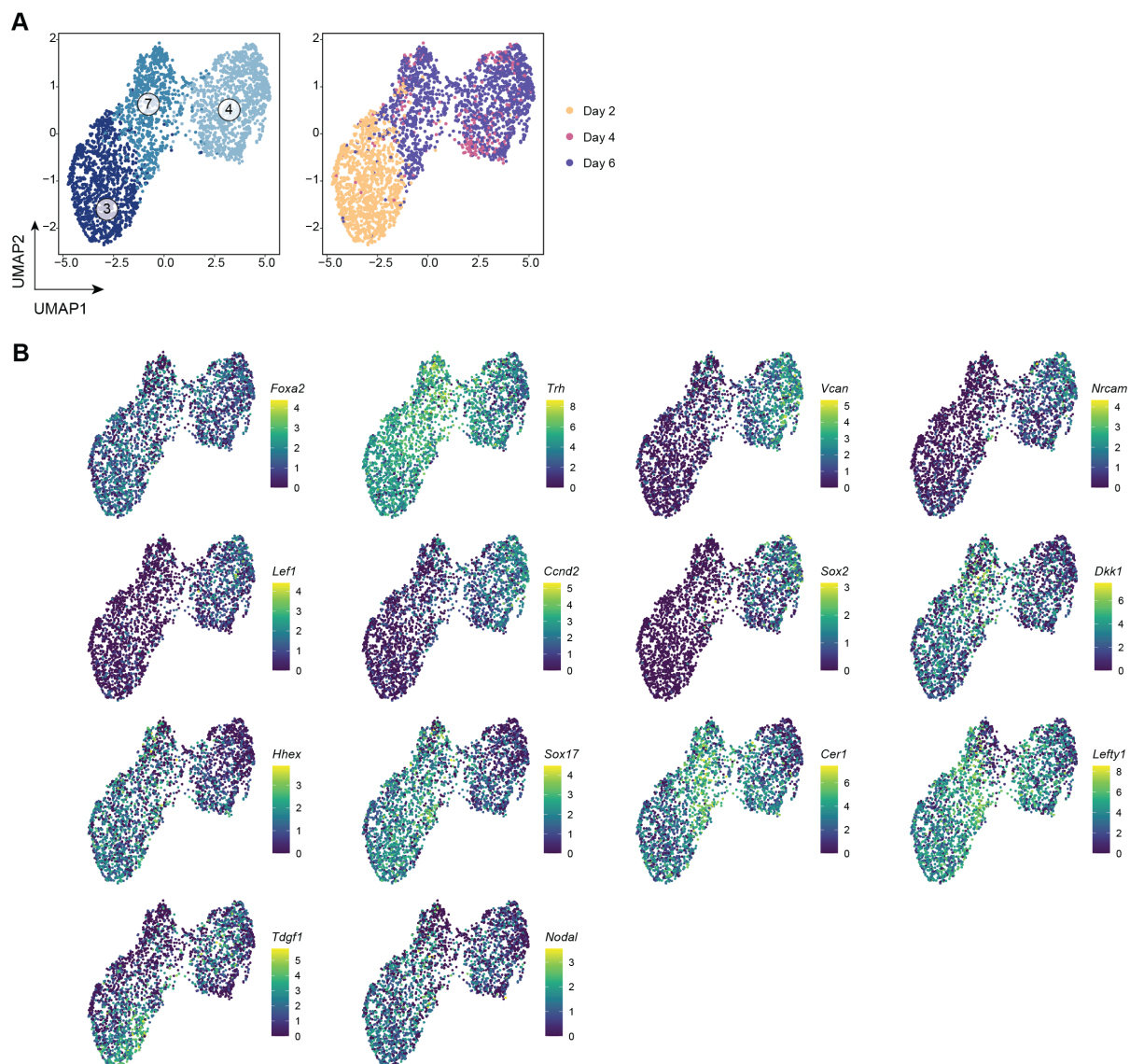
Supplementary Figure S12: (A) UMAP of definitive endoderm, colored by clustering results (left) and sampling day (right). (B) UMAP visualisations of 14 selected markers of clusters.

Supplementary Figure S13: (A) UMAP of epiblast, colored by clustering results (left) and sampling day (right). (B) Violin plots showing the RNA expression of 12 selected markers. (C) UMAP visualisation of 4 selected TF, higlighted by the motif enrichment scores derived from ATAC using chromVar (top row) and RNA expression (bottom row).
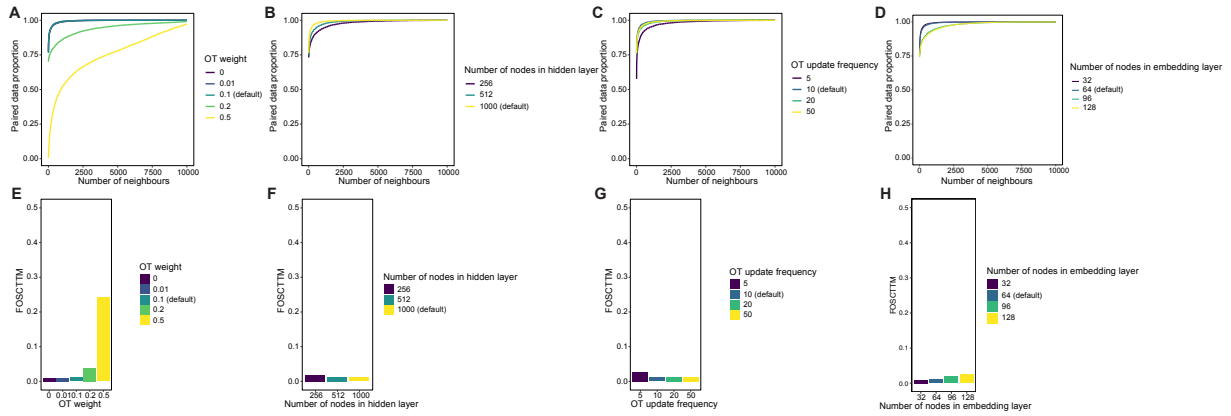
Supplementary Figure S14: Robustness of scTIE with respect to the tuning parameters in modality alignment. (A-D) Proportion of ground truth pairs within certain number of nearest neighbors (higher is better), with different (A) OT weight; (B) Number of nodes in hidden layer; (C) OT update frequency; (D) Number of nodes in embedding layer. (E-H) Barplots of FOSCTTM (fraction of samples closer than the true match, lower is better) values, with different (E) OT weight; (F) Number of nodes in hidden layer; (G) OT update frequency; (H) Number of nodes in embedding layer.
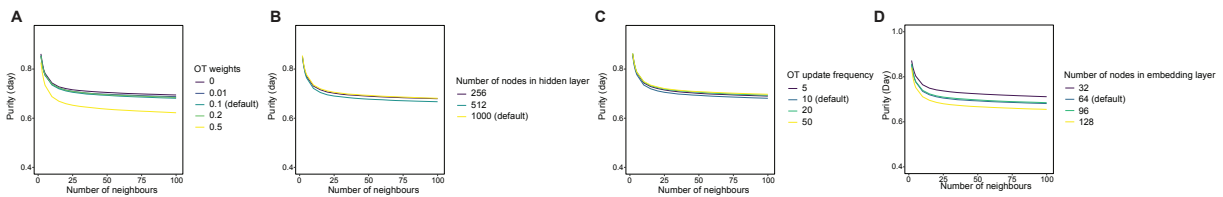

Supplementary Figure S15: Robustness of scTIE with respect to the tuning parameters in time point alignment. Average purity scores of sampling days based on different number of neighbors (lower values indicate better mixing), with different (A) OT weight; (B) number of nodes in the hidden layer; (C) OT updating frequency; (D) Number of nodes in embedding layer.

12
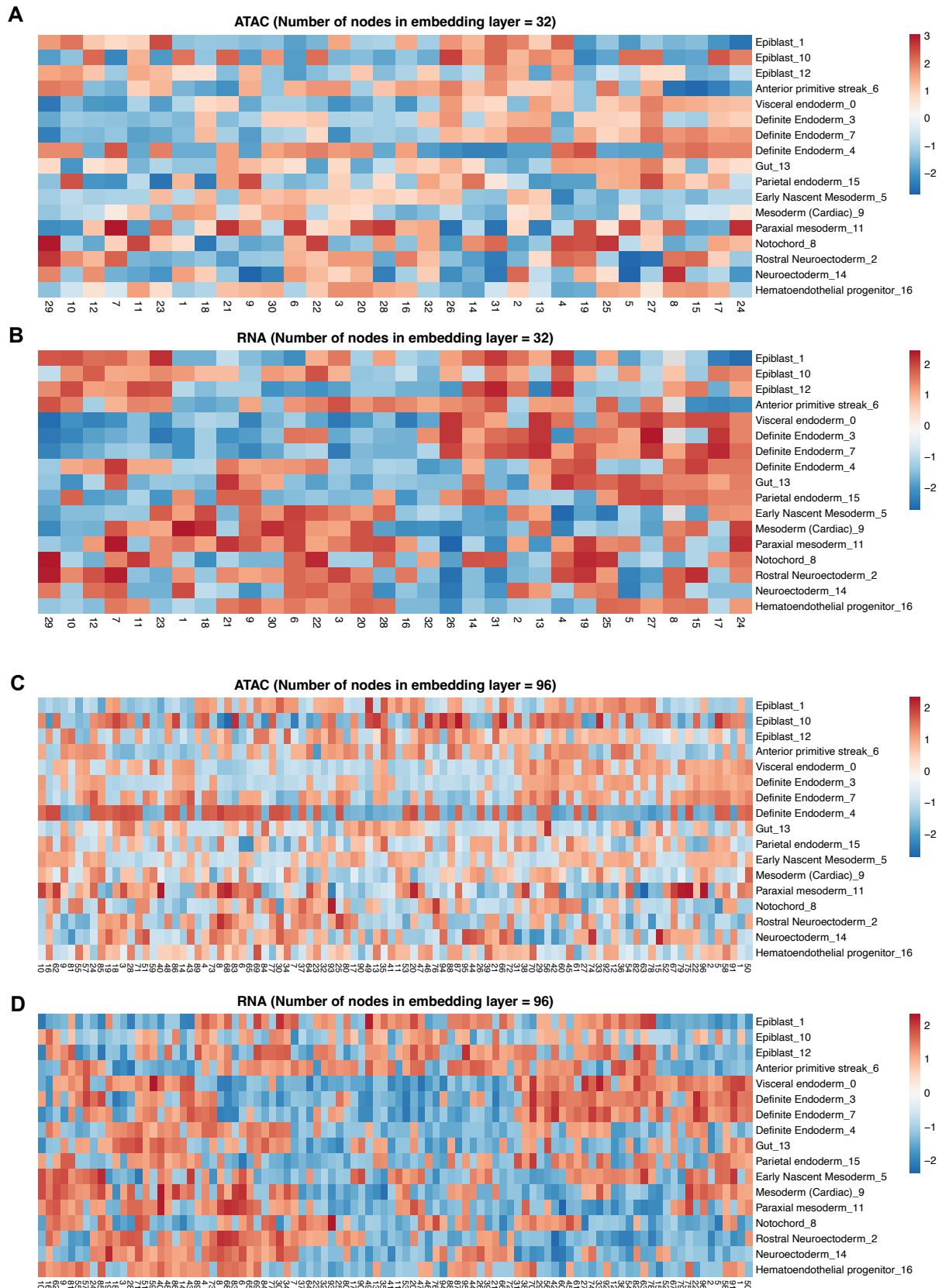
Supplementary Figure S16: Enrichment scores of the gradient ranking in each embedding dimension with the number of nodes in the embedding layer set as (A-B) 32 and (C-D) 96 using the ATAC (A, C) and RNA (B, D) marker list for each cell type.
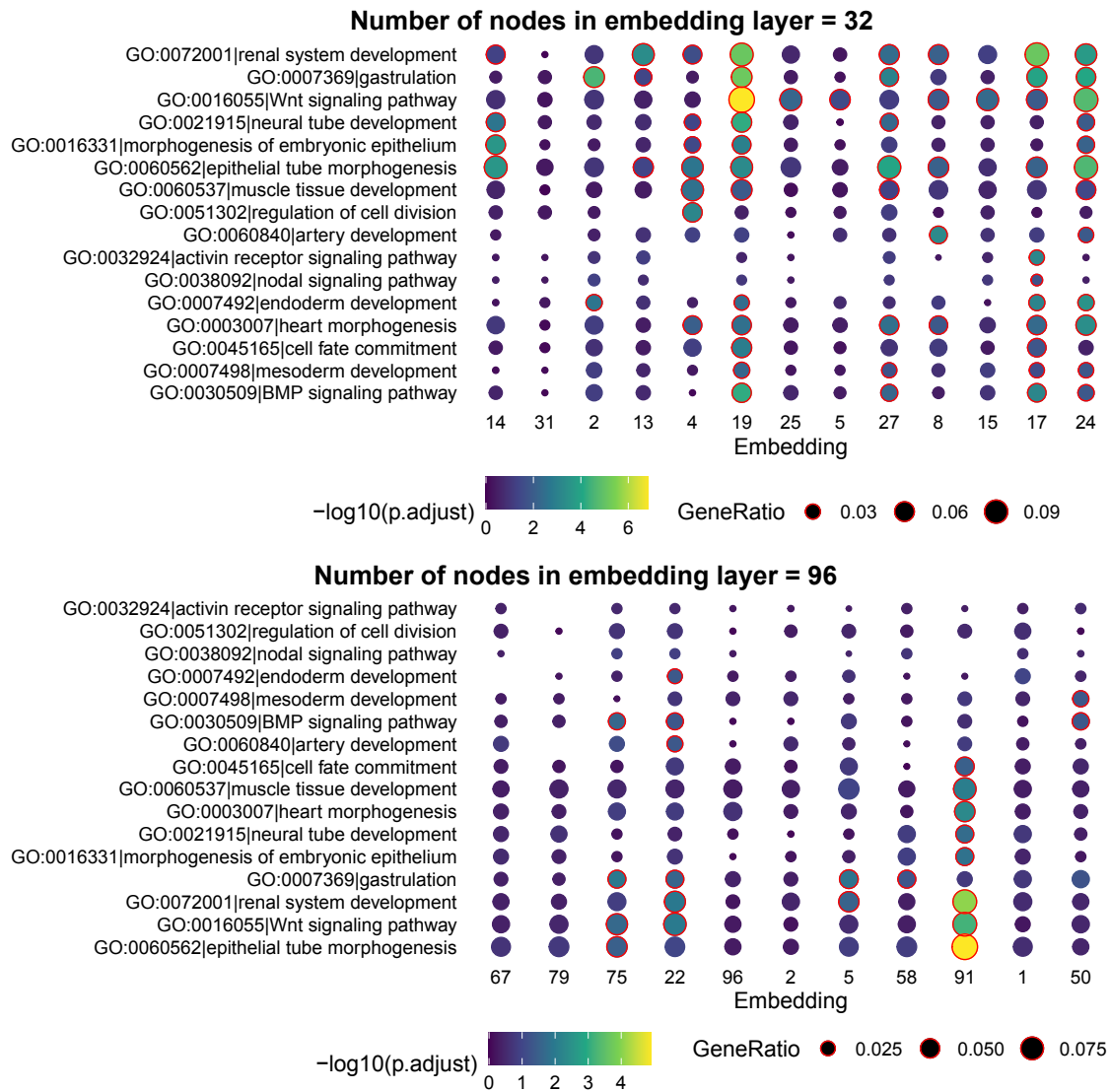
Supplementary Figure S17: Gene ontology enrichment of selected pathways on the gradient ranking of a subset of embedding dimensions with the number of nodes in the embedding layer set as 32 (top panel) and 96 (bottom panel).
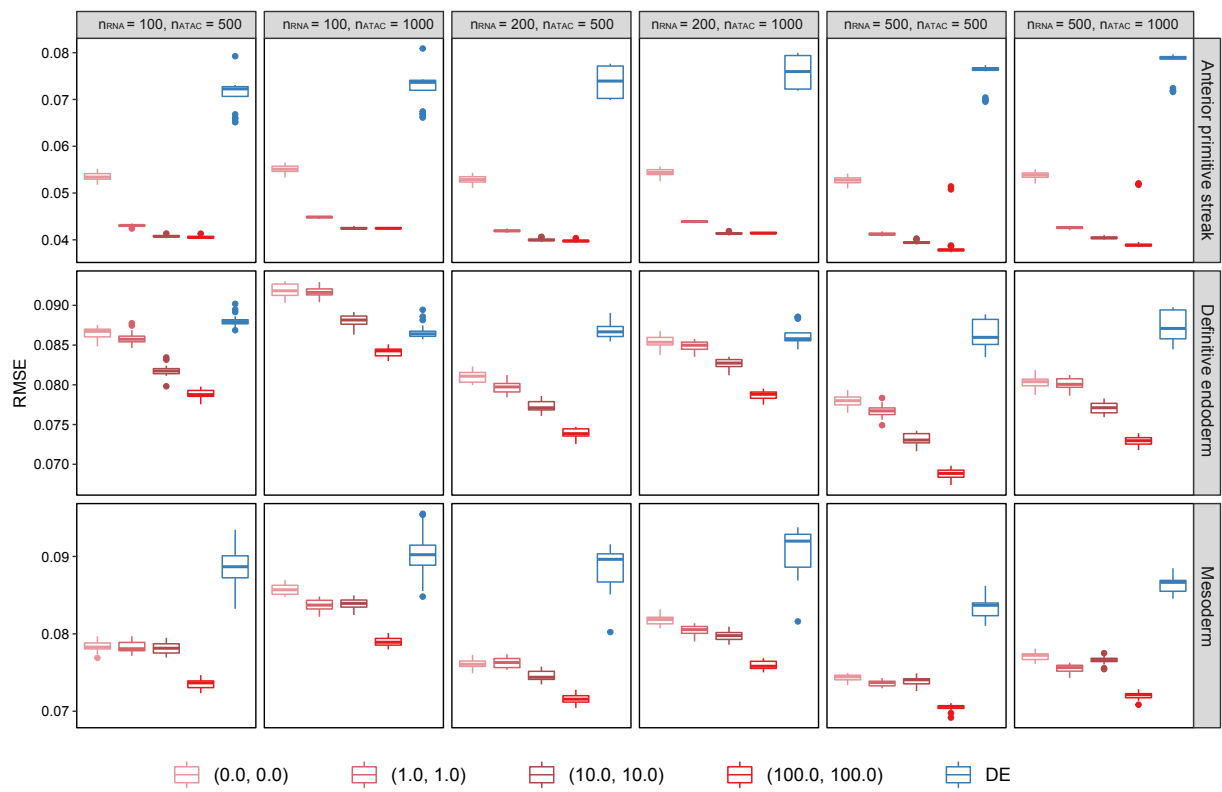
Supplementary Figure S18: Evaluation of transition probability predictions for three different cell fates: anterior primitive streak, definitive endoderm and mesoderm, comparing (1) different number of genes/peaks; (2) different L1 regularization weights used in the prediction task.
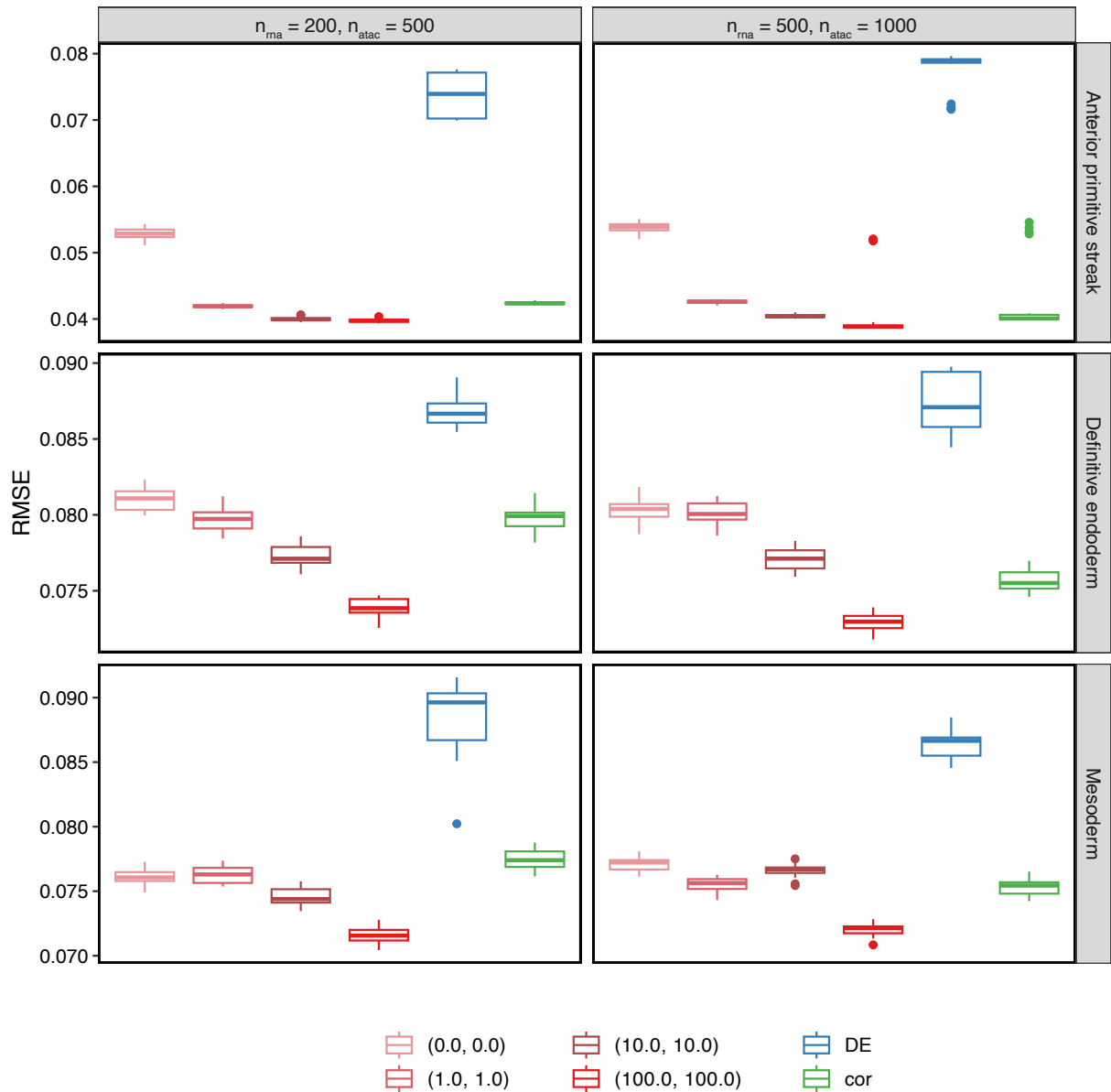
Supplementary Figure S19: RMSE of transition probability predictions for three different cell fates: anterior primitive streak, definitive endoderm and mesoderm, comparing (1) different number of genes/peaks; (2) different L1 regularization weights used in the prediction task against DE/DA analysis and the correlation method.
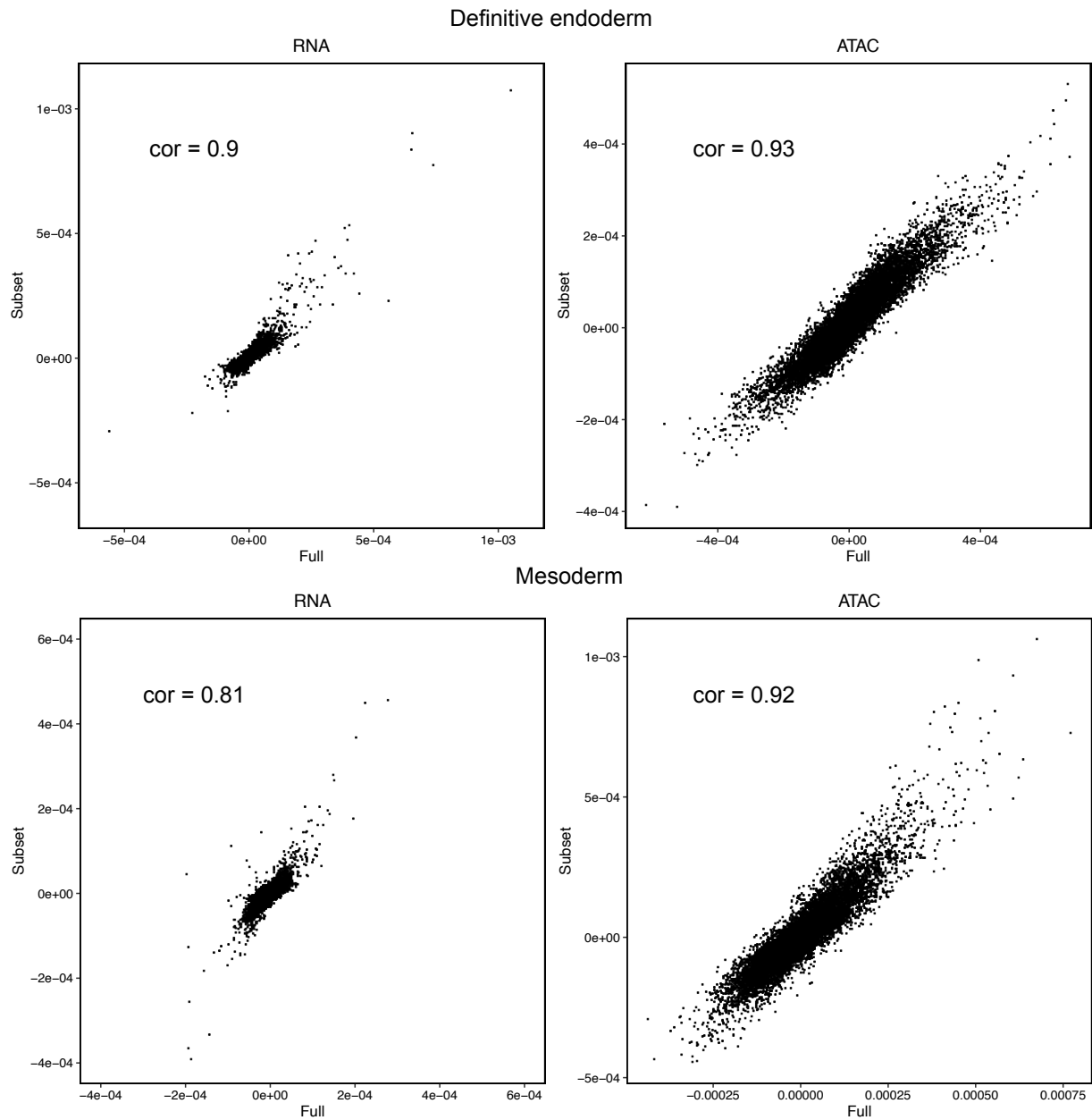
Supplementary Figure S20: Scatter plots comparing the feature gradients derived from the full data (x-axis) vs. subset data (y-axis) for two lineages: definitive endoderm (first row) and meso-derm (second row).
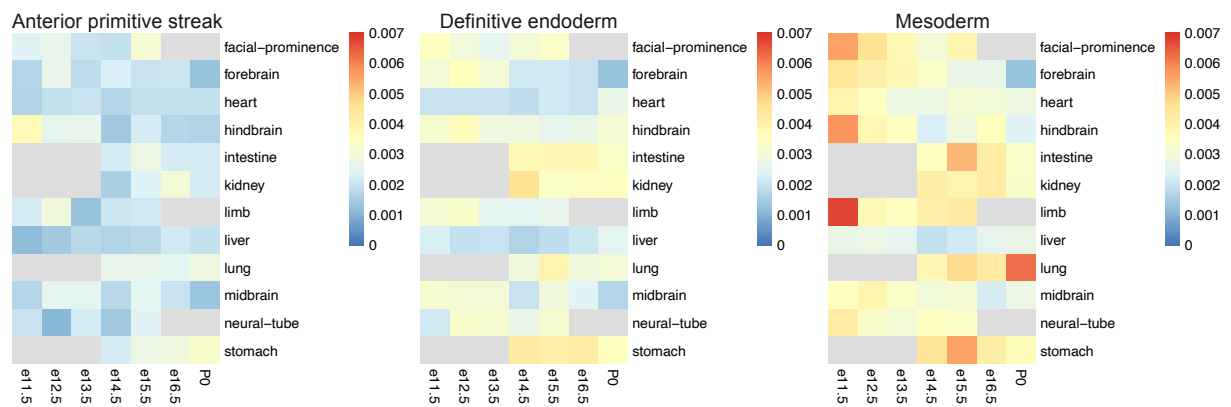
Supplementary Figure S21: Similarity of top DA regions with enhancers of 12 tissues at seven developmental stages from known enhancer databases.
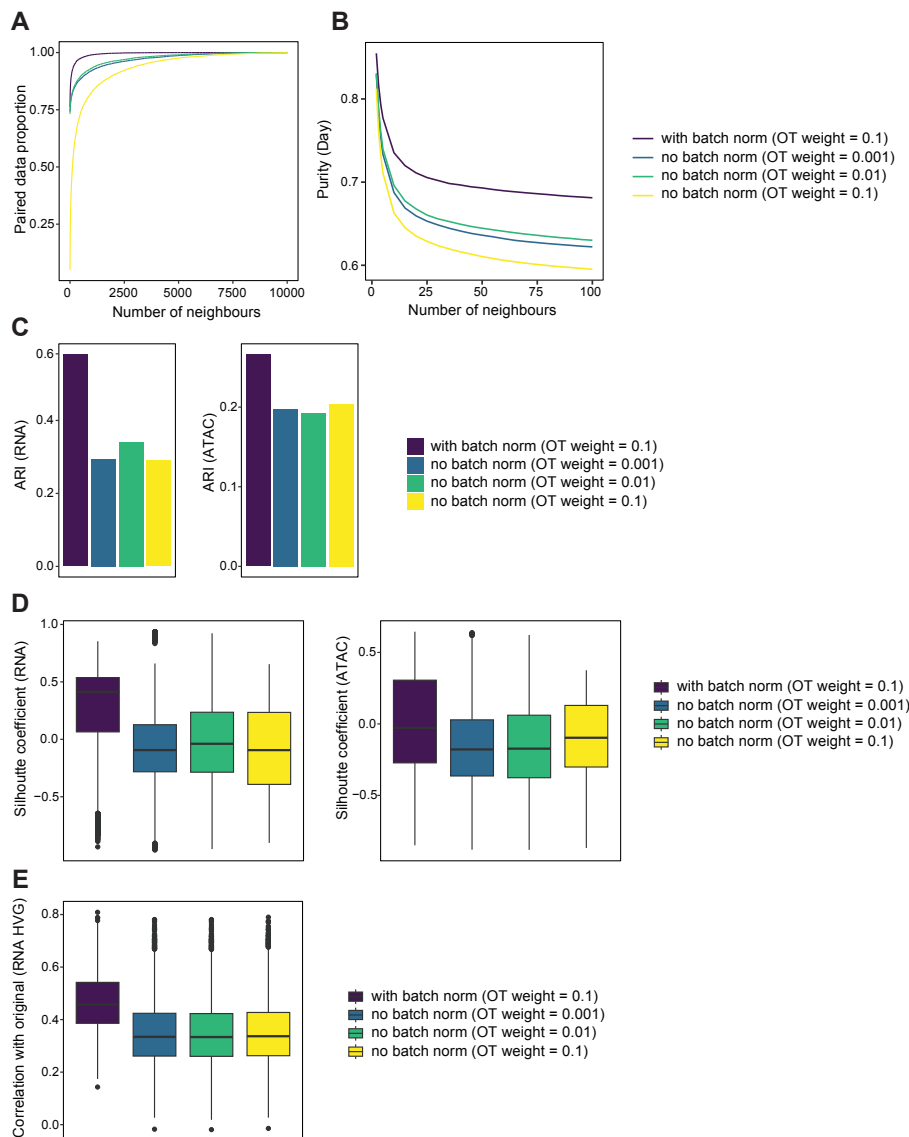
Supplementary Figure S22: scTIE performance comparison with and without the coupled batch norm layers in RNA: (A) Proportion of ground truth pairs within a given number of nearest neighbors; (B) Average purity scores of sampling days based on different numbers of nearest neighbors; (C) The bar plots show the ARI values comparing the clustering from different settings of scTIE with the clustering on RNA (left) and ATAC alone (right); higher values indicate better agreement. (D) Box plots show the silhouette coefficients comparing the clustering from different settings of scTIE based on distance matrices computed from the RNA (left) and ATAC (right) UMAP coordinates. Higher values indicate better agreement. (E) Correlation of scTIE reconstructed RNA expression with the original RNA expression of highly variable genes (HVG).
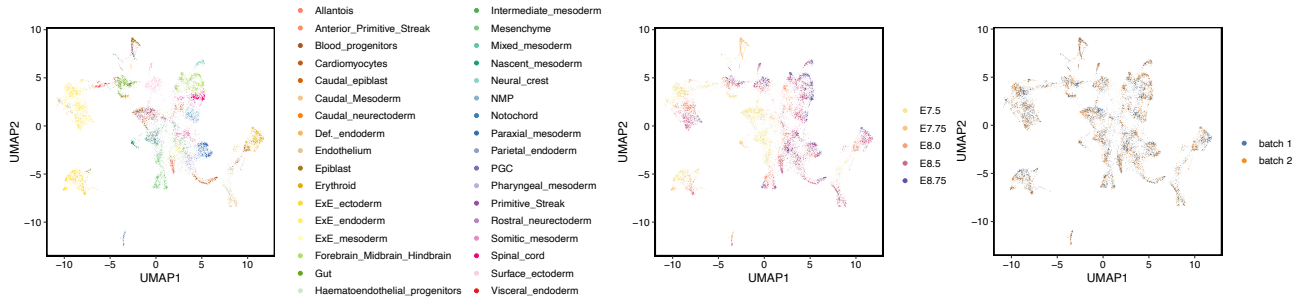
Supplementary Figure S23: UMAP of RNA embeddings from the pre-trained RNA model on a synthetic dataset with batch effects in both RNA and ATAC data.
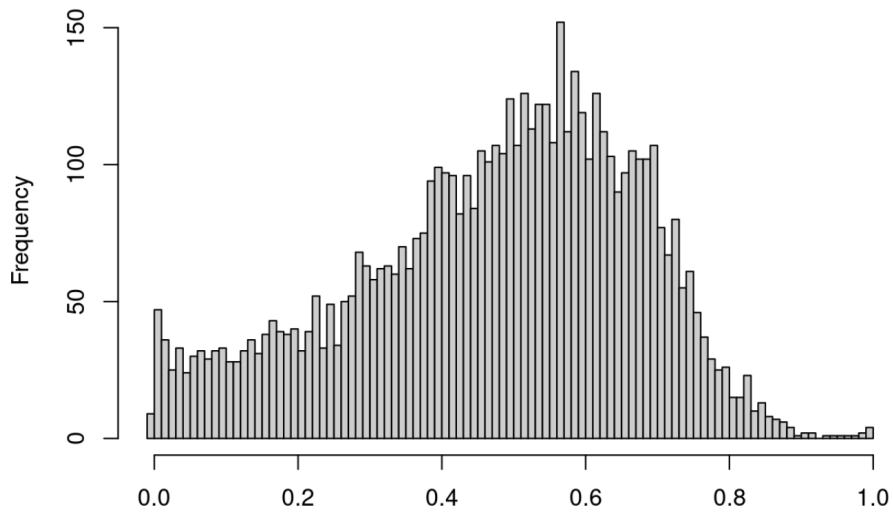
Supplementary Figure S24: Correlation between the two ways of gamma matrix estimation.

	Gradient ranking	DE ranking	DE adj p-value
Sox17	126.00	1252.00	0.46
Smad3	260.00	2074.00	0.81
Zic3	150.00	1317.00	0.49
Twist1	441.00	184.00	0.00
Nfat5	368.00	2197.00	0.84
Hhex	393.00	2650.00	0.98

Table S1: Comparison of the gradient rankings, DE rankings and adjusted p-values under DE for key TFs in mesoderm lineage.